Braz J Phys (2014) 44:346–355
DOI 10.1007/s13538-014-0236-4

CONDENSED MATTER

Structure and Morphology of SBA-15 Thin Films on Different Substrates

Silvanna L. A. Maranhão · Luis C. Cides da Silva · Alexandre F. Michels · Flavio Horowitz · Jivaldo R. Matos · Márcia C. A. Fantini

Received: 22 May 2013 / Published online: 17 June 2014

Abstract Well-ordered hexagonal mesoporous silica thin films, SBA-15 type, were synthesized with Pluronic P123 and tetraethyl orthosilicate in a diluted ethanol-hydrochloric acid solution. Films deposited on a broad range of distinct substrates by a sol-gel dip-coating method resulted in transparent and adherent samples. Transmission electron microscopy images revealed, predominantly, well-ordered regions of hexagonal arrays of cylindrical mesopores parallel to the substrate. X-ray reflectivity showed similar lattice parameters for all analyzed films, with a (*h00*) preferred orientation. The films presented diverse shrinkage susceptibilities, which were tested after different polymer removal procedures. Calcined films have 342 m^2/g surface area, 0.130 cm^3/g pore volume, and 6.8 nm pore diameter. The wetting characteristics of the substrates in water and alcoholic solutions were evaluated. The films showed different structural properties, mostly related to the mean surface roughness of the substrates and to the drying process.

Keywords SBA-15 · Thin film · Sol-gel · Dip coating

S. L. A. Maranhão · M. C. A. Fantini (✉)
Instituto de Física da, Universidade de São Paulo, CP 66318, São Paulo, SP 05315-970, Brazil
e-mail: mfantini@if.usp.br

S. L. A. Maranhão
e-mail: silvanna.maranhao@gmail.com

L. C. Cides da Silva · J. R. Matos
Instituto de Química da, Universidade de São Paulo, CP 26077, São Paulo, SP 05599-970, Brazil

L. C. Cides da Silva
e-mail: lccides@iq.usp.br

J. R. Matos
e-mail: jdrmatos@gmail.com

A. F. Michels · F. Horowitz
Instituto de Fisica, UFRGS, Campus do Vale, CP 15051, Porto Alegre, RS 91501-970, Brazil

A. F. Michels
e-mail: michels@if.ufrgs.br

F. Horowitz
e-mail: flavio.horowitz@ufrgs.br

1 Introduction

Nano-scaled materials have become the basis of advanced new technologies. Among them, mesoporous-ordered materials suit application in various branches demanding high technology. Found in several macroscopic morphologies, such as spheres [1], rods [2], and films [3], and displaying many interesting properties [4], these materials were promoted and popularized by Mobil Oil Corporation [5, 6]. Unfortunately, the use of cationic surfactant templates in an alkaline condition in their syntheses leads to mesostructures with thin walls and limited hydrothermal stability. An early improvement was achieved by Huo and co-workers [7], who reported that mesophases are formed by metal oxides and cationic/anionic surfactants, under a wide range of pH conditions. In 1998, another advance was made when triblock copolymer was used to prepare, under an acid condition, the mesoporous silica named SBA-15, with periodic 5 to 30 nm pores, thick walls, and greater hydrothermal stability [8]. Due to their biodegradability, low cost, and non-toxic properties, block copolymers have been frequently used as templates for the assembly of well-ordered mesoporous silicas. In a typical synthesis, aggregation of the template into a micellar array is followed by addition of the silica source. During hydrolysis and evaporation of volatile molecules, the silica molecular sieve is formed. To remove the template and obtain a porous material, calcination at a relatively high temperature (~500 °C) is commonly used. Alternatively, the template can be extracted in a solvent, a procedure that allows recovery and

reuse. No structural destruction is observed, and pores of specific shapes can be created [9–11]. The most studied silica mesoporous materials have cubic, lamellar, or hexagonal structures and are usually prepared as powders. These mesoporous materials are of interest in industry as catalyst supports, adsorbents, drug delivery nanocarriers, and hosts in host-guest chemistry [12–14].

The deposition of ordered mesoporous silica films is also a field of vast scientific interest [15]. These films can be made by an aerogel/xerogel process [16], but better controlled porosity, pore size distribution, film-structure organization, and reproducibility are generally obtained by combining a sol-gel method with self-assembly of organic templates. The film formation during dip coating is dynamic and involves rapid solvent evaporation, mesophase formation, and polycondensation of the inorganic entities, a mechanism elucidated by Lu and co-workers [17]. Self-assembly is driven by evaporation during film deposition, and thin-film mesophases are quickly formed. This synthesis strategy, named evaporation-induced self-assembly (EISA) [18, 19], has been widely used to prepare mesoporous films. Zhao et al. [20] prepared the first mesoporous films using cetyltriethylammonium bromide (CTAB) by dip coating on solid substrates. Nishiyama et al. [21] also used CTAB to form MCM-48 mesoporous films on stainless steel.

More recently, Alberius and co-workers [22] prepared a well-ordered mesostructured silica and titania films using poly(ethylene oxide)-poly(propylene oxide)-poly(ethylene oxide) triblock copolymer species (Pluronic P123) as the structure-directing agents. Yao and co-works [23] showed that mesoscopic order is detected by nucleation of ordered regions in thin films grown at air-water interfaces, after the induction period. Then, regular packing via ordering of disordered regions within the film occurs. Grosso et al. [24] demonstrated that the organization depends mostly on the chemical composition of the film at the modulable steady state (MSS), generally attained seconds after the drying line. The control of mesophase ordering and, therefore, of macroscopic morphology is fundamental for certain technological applications, such as microelectronics, sensors, and membranes [17, 25, 26].

The orientation of the nanoscopic domain depends on the degree of silica condensation, concentration of surfactant, and dipping rate. Miyata and Kuroda [27] prepared a film by an epitaxial-like growth, in which the substrate faces down the reactant acid solution containing tetraethyl orthosilicate (TEOS) and a cationic surfactant. They reported that the alignment of the mesochannels in the mesostructured silica films is affected by interactions at the film/substrate interface and found that the (110) silicon surface provides the best results. Later, the same authors showed the formation of mesoporous silica films with fully aligned mesochannels onto a substrate formed by rubbing a polyimide spin-coated layer onto a clean silica glass [28].

Chougnet et al. [29] compared the ordering of cylindrical and compact hexagonal mesoporous films deposited by spin coating on dielectric and metallic substrates and on a modified glass, grafted with statistical copolymers containing different ethylene oxide fractions. The diffraction patterns revealed template- and substrate type-dependent film contractions, which were enhanced when a block copolymer was used. They concluded that the similar chemical natures of the template molecules and modified glass fasten the structure formation and enhance the contraction of the ordered structure. In a recent work, Chougnet et al. [30] studied the same films on glass, silicon, and metal substrates and demonstrated, by diffraction patterns, that chemical (surface interaction) and physical (roughness) properties influence the formation of the ordered structure and noted that additional study will be necessary to de-convolute the roles of the relevant parameters. Many authors pointed out that the film structure and morphology depend on the deposition method, the substrate type, and the state [17, 29–38]. For example, as an attempt to avoid the influence of the substrate on film structure, Bandyopadhyaya et al. [38] developed a transferable-film synthesis route and produced the MCM-41 type of films. A complete review on synthesis, structure, and applications of mesoporous and macroporous films was published by Guliants et al. [39].

As far as our knowledge goes, no detailed work focused on the substrate properties analyzes SBA-15 type-ordered mesoporous silica films on different substrates, deposited under identical conditions. This work focuses on the influence of the substrate characteristics, such as hydrophilic/hydrophobic nature and surface roughness, upon the pore size, lattice parameter, and mesoscopic order of silica dip-coated films, prepared by a sol-gel synthesis. Our goals in this research were to deposit and characterize well-ordered hexagonal mesoporous silica (SBA-15) thin films onto various substrates and to examine the film structure and morphology as well as the effects of different template removal procedures on the film structural properties. It was not our purpose to optimize the deposition of the films onto the different substrates to achieve identical morphological features, for example, by means of sophisticated or novel surface treatments. Instead, we treated all the substrate surfaces with the same, standard cleaning process and evaluated the structure of the films deposited on them.

2 Experimental

2.1 Substrates

Before coating, the glass, steel, single-crystalline (100) silicon, plastic, and Kapton polyimide substrates were first washed with water and detergent. They were then cleaned,

in sequence, with acetone, isopropanol, and distilled water, in an ultrasonic bath and, finally, dried at 100 °C.

Contact angle measurements were performed in order to investigate the influence of the hydrophilicity/hydrophobicity of each substrate on the SBA-15 film structure. The sessile drop method was used. A drop of the liquid (water or ethanol/HCl/water solutions used to prepare the SBA-15 sol) was deposited on a horizontal surface and observed in a cross section. The static contact angle at the liquid-solid interface was measured immediately after the sample-cleaning process. A micro-syringe was used to deposit a 4- to 6-μL droplet of de-ionized water, or of the SBA-15 sol, onto the substrate surface. The drop was observed directly with a microscope objective, and its image was digitally captured by a 1.4-megapixel digital CCD camera, interfaced with and controlled by a microcomputer. The droplet was imaged by an Olympus BX-41 microscope objective lens, and the image data was processed by the Surftens AutoCAD software, which determines the liquid-solid interface contact angle. The surface roughnesses of the substrates were analyzed by atomic force microscopy (AFM) using a PicoSPM I microscope (Molecular Imaging) with a PicoScan 2100 (Molecular Imaging) controller, operating with around 1-Hz sweeping speed, with 256 points per line. The glass, steel, (100) silicon, and Kapton substrates were analyzed in AFM contact mode with a rectangular silicon cantilever (Nanosensors). For the plastic substrate, the MAC Mode (Molecular Imaging) with a MACLever of type II cantilever (Molecular Imaging) was used.

2.2 Syntheses

Mesoporous silica was templated using the non-ionic triblock copolymer Pluronic P123 (EO_{20} PO_{70} EO_{20}) from BASF and tetraethyl orthosilicate (TEOS, 98 % Aldrich) as the silica source in a diluted hydrochloric acid solution (HCl), following sol-gel synthesis [22]. In a typical preparation procedure, under vigorous agitation, 10.4 g of TEOS was prehydrolyzed in a solution containing 5.4 g of HCl (pH=2) and 12 g of ethanol, at room temperature. After 20 min of stirring, this solution was mixed with a solution containing the triblock copolymer P123 dissolved in 8 g of ethanol. The amount of 45 % vol. of the copolymer was chosen to produce the desired hexagonal morphology. The final solution was stirred for 3 h.

A dip-coater was used to deposit the films onto the substrates [glass, Kapton, single-crystalline (100) silicon, stainless steel, and commercial plastic "high temperature cook wrap"] at 6 cm/min rate. The deposited films were subsequently maintained at 40 °C for 24 h to dry and to complete the silica polymerization. Finally, the polymer template was removed either by heating at a 1 °C/min rate to 400 °C under nitrogen flow and holding for 4 h, which yielded transparent adherent films, or by solvent extraction in ethanol flow. Since Kapton and plastic degrade at 400 °C, the films deposited on these two substrates were not calcinated.

Since the framework-surfactant interactions in mesoporous materials involve electrostatic and hydrogen-bonding interactions, liquid extraction is an option for removing the copolymer surfactant species. This procedure yields intact silica films and allows recovery and reuse of the organic species [9–11]. The solvent extraction of the templated silica sol-gel films was performed in a reflux with ethanol at 80 °C for 12 h. The films were then washed with ethanol and dried at room temperature.

2.3 Characterization

The film thickness was measured with an Alpha-Step 500 Surface Profiler (10-nm precision), using a sharp step between the films and substrates, which was made with a mask during deposition. Self-sustained films were obtained by a pop-off technique, using samples prepared on glass or stainless steel surface. These films were collected on a copper grid and examined in a transmission electron microscope (TEM) LEO 906E at 100 kV.

A thick film was deposited on a large glass substrate, dried at room temperature, and scratched from the surface. The resulting powder was calcined at 673 K for 4 h. This sample was prepared because a large amount of material is necessary to measure the nitrogen ad-(de)sorption isotherm. The data were taken at 77 K on a Quantachrome Nova volumetric adsorption analyzer. Before the adsorption measurements, the samples were outgassed at 473 K. The isotherms were used to evaluate the Brunauer-Emmett-Teller (BET) specific surface area, pore volume, and pore size.

X-ray reflectometry (XRR) patterns were obtained over the $0.6° < 2\theta < 4.0°$ with CuKα radiation (λ=0.15418 nm) for films deposited on glass, (100) silicon, and stainless steel. This angular range was chosen because it contains the Miller indices generally detected in mesoporous films [22]. In contrast with powder samples, thin films usually present texture and only one family of diffraction planes. The lattice parameter is therefore calculated from these available data.

Small-angle X-ray scattering (SAXS) measurements were carried out by transmission, using line focus geometry on films deposited over plastic and Kapton polyimide. The films were packed in ten foils in order to increase the scattering intensity. The system was collimated by slits, with a vacuum path between the sample and the detector. The wavelength of the copper monochromatic X-ray beam was λ=0.15418 nm, and the intensity was recorded for 12 h with a power of 10 kW (50 kV, 200 mA) in an image plate detector.

3 Results and Discussion

The contact angles on Table 1 represent averages of several values obtained on different areas of each substrate surface.

Table 1 Contact angles and roughness of each substrate

Substrate	Water contact angle/°	SBA-15 sol contact angle/°	Rms (roughness)/nm
Glass	35±2	<3	2.12
Kapton	53±2	2±2	0.21
Silicon	56±2	<3	0.53
Stainless steel	67±2	<3	8.14
Plastic	70±2	3±2	1.40

Different results were obtained from surfaces of the same materials before cleaning and after pre-cleaning. The hydrophilic/hydrophobic properties varied widely from material to material, glass being the most hydrophobic one. While all substrates have high affinity to acidic alcoholic sol, plastic and Kapton are the ones with less affinity, an indication that the drying process is slower on these two substrates. All these data corroborate the notion that the substrates have similar chemical interaction when in contact to the ethanol deposition sol. We therefore expect the wetting properties of the substrates not to drastically influence the structure of the mesoporous films. Since surface imperfections may also influence the contact angle and the film morphology, we have also analyzed the surface roughness of our substrates. The mean surface roughnesses of the substrates (rms) shown by the AFM images in Fig. 1a–e were evaluated by the equipment software.

The Kapton and (100) Si substrates are the flattest surfaces, showing 0.21 and 0.53 nm rms, respectively. Plastic and glass present 1.40 and 2.12 nm rms, respectively, and the stainless steel substrate has the largest rms, 8.14 nm. Since the roughnesses of all substrates are smaller than 10 nm, we expect the contact angle not to depend on them. The contact angle measurements with the water and the sol presented no correlation to the substrate roughness, as evidenced by the results in Table 1. These results will be compared to the XRR, SAXS, and TEM data, since different structural properties were observed for films on the five surfaces.

The resulting mesoporous silica films, deposited on the different substrates, exhibit transparence and efficient adherence. The films are not easily removed from the substrates when scratched. In all substrates, the film surface is flat under naked eye inspection as well as under 400× optical

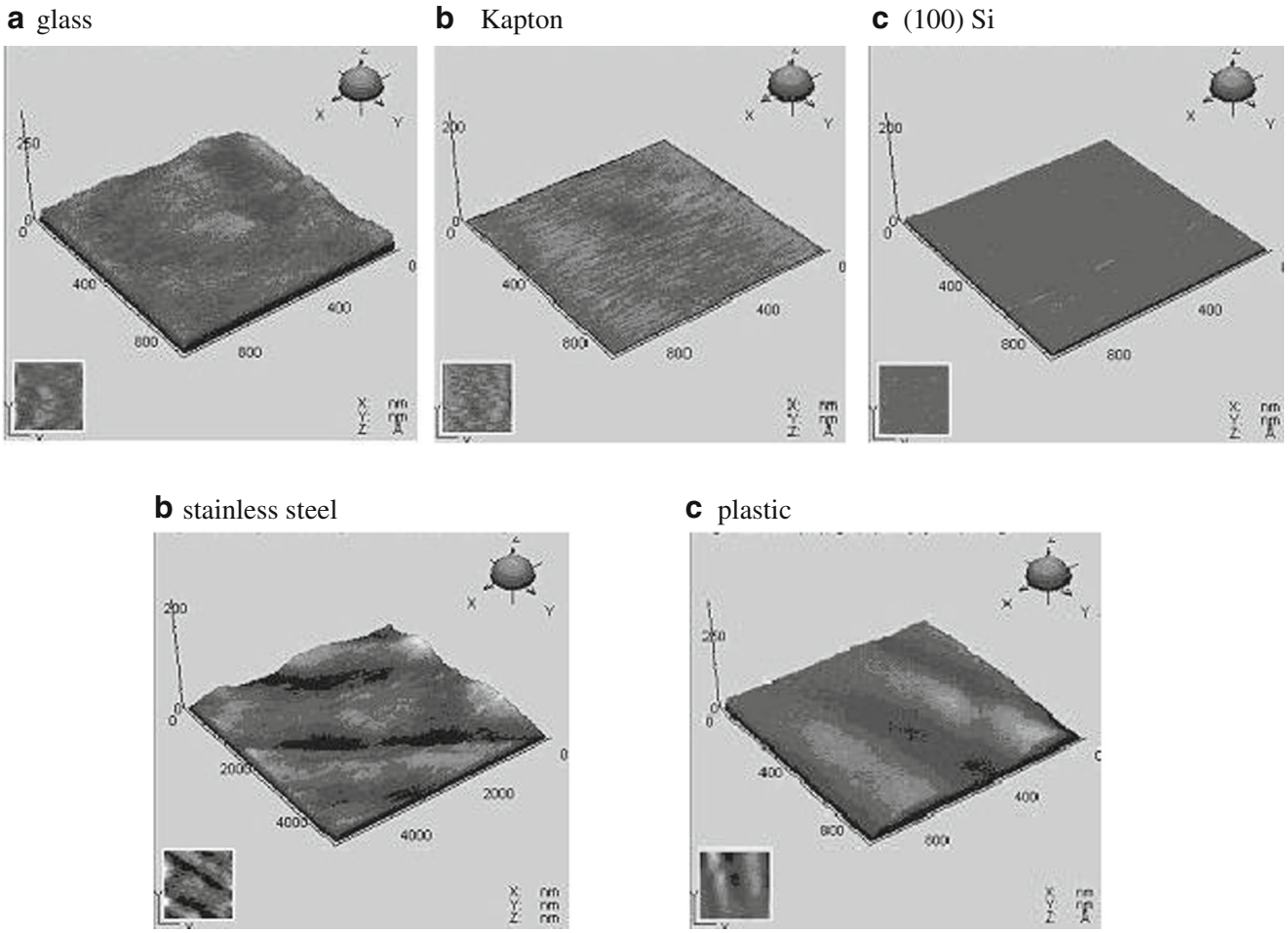

Fig. 1 Substrate surfaces measured by atomic force microscopy (AFM): **a** glass, **b** Kapton, **c** silicon, **d** stainless steel, and **e** plastic

magnification. The thickness of as-synthesized films on glass, steel, and silicon was between 400 and 600 nm (one-dip process); it was between 250 and 450 nm for calcined films and between 300 and 500 nm for films washed in ethanol. Films deposited with five dips can reach a thickness of around 2.5 μm.

A common characterization technique of porous powdered materials is gas adsorption, which yields the specific surface area, pore volume, and pore size distribution. A few papers on thin mesoporous silica films have reported the analysis of pore accessibility by means of a surface acoustic wave technique [17, 40], N_2 gas adsorption measurements applied to powder samples scratched out of the substrate surface [41, 42], ellipsometry [43], X-ray scattering [44], and X-ray reflectometry [45] together with N_2 adsorption. The results concerning the BET surface area (S_{BET}), pore volume and diameter depend on the template and symmetry of the mesostructure. Typical S_{BET} values ranging from 100 to 1,000 m^2/g and pore diameter from 4 to 8 nm have been achieved. We have obtained an S_{BET} of 342 m^2/g, a pore volume of 0.130 cm^3/g, and a mean diameter of 6.8 nm. Figure 2a depicts the isotherm of the calcined scratched powder, and Fig. 2b presents the SAXS data of the same sample with and without the template. All these results are in accordance with XRR, SAXS, and TEM data from the films.

Figure 3 shows the XRR patterns of the SBA-15 films deposited on a glass slide. For the as-synthesized sample, the (100) and (200) reflections give a lattice parameter a= 11 nm of the hexagonal bi-dimensional *p6mm* symmetry. Calcination yields a pattern in which the same reflections yield a smaller lattice parameter, a=8.0 nm, which indicates structural shrinkage. The film washed in ethanol yields peaks corresponding to the lattice parameter a=8.6 nm, larger than the result for the calcined film. The two weak peaks at

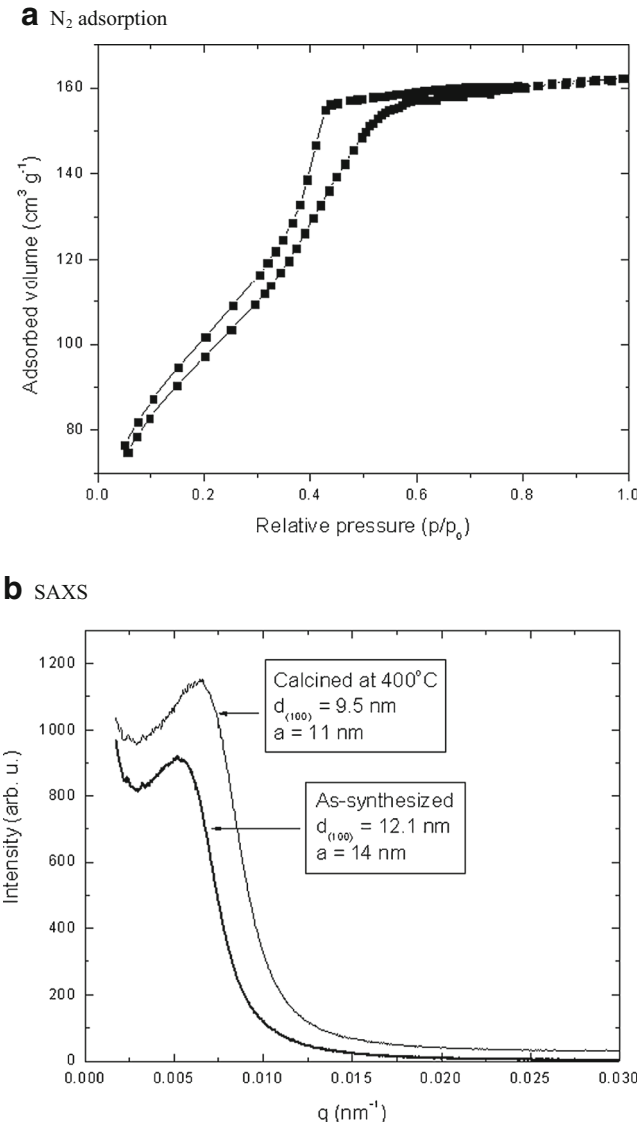

Fig. 2 **a** N_2 adsorption isotherm and **b** SAXS of the SBA-15 powder scratched from a thick film deposited on a large glass surface

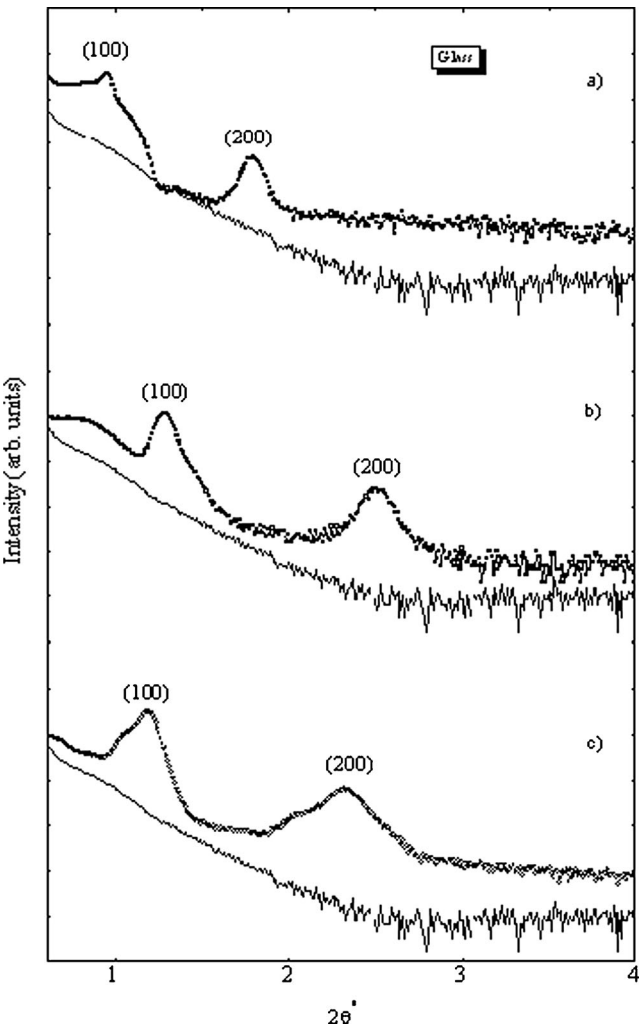

Fig. 3 XRR patterns of SBA-15 film on glass: **a)** as-synthesized: *full square* and glass substrate: *line*; **b)** calcined: *empty square* and glass substrate: *line*; **c)** template extraction with ethanol: *empty circle* and glass substrate: *line*

2 θ=1.03° and 2.03° nonetheless show that the template was not fully removed.

For films deposited on stainless steel, Fig. 4, the XRR patterns display less well-resolved peaks. For the as-deposited film, this result is due to the rough stainless steel substrate covered with polymeric material, which avoids perfect alignment of the sample in front of the X-ray beam and promotes absorption. After polymer removal for the same sample, a higher electronic density contrast is observed, as frequently reported in the literature [46], and there is less absorption. The influence of the substrate topography on the structural properties of mesoporous SBA-16 films has also been reported for samples deposited on glass covered by indium tin oxide (ITO) [37]. The diffraction of an as-synthesized SBA-15 film presented only the (200) peak and a broad band after calcination. Well-defined peaks were obtained only from the film submitted to template extraction with ethanol, with a=8.6 nm lattice parameter. Nevertheless,

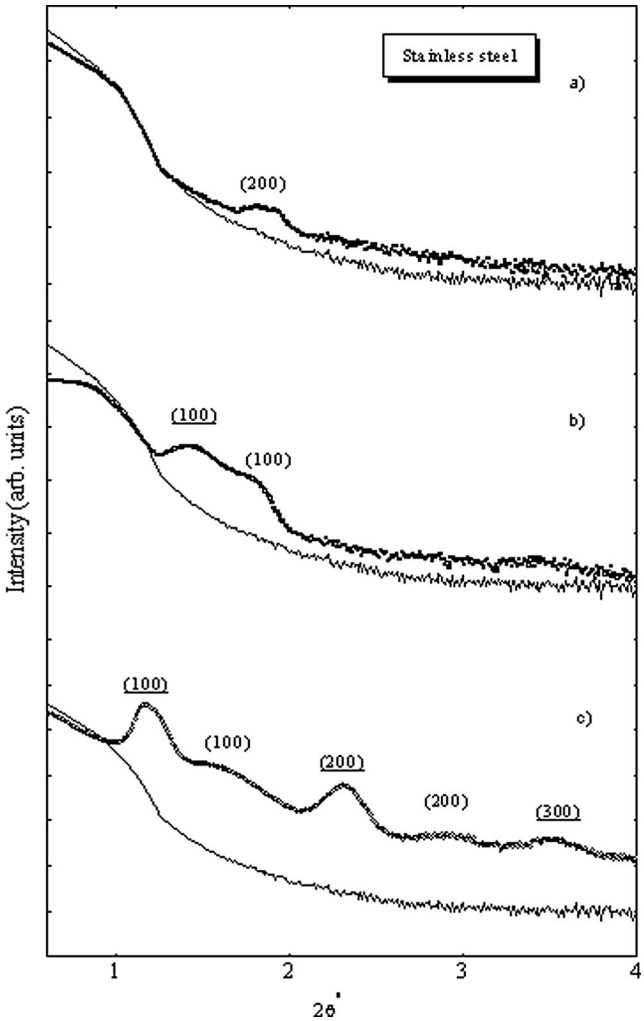

Fig. 4 XRR patterns of SBA-15 film on stainless steel: **a**) as-synthesized: *full square* and stainless steel substrate: *line*; **b**) calcined: *empty square* and stainless steel substrate: *line*; **c**) template extraction with ethanol: *empty circle* and stainless steel substrate: *line*

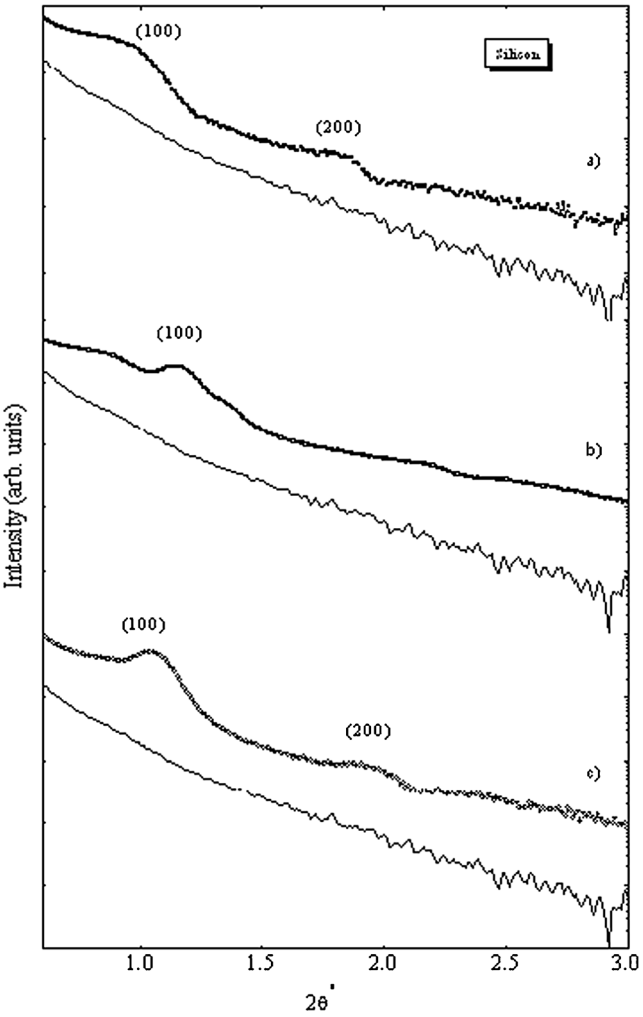

Fig. 5 XRR Patterns of SBA-15 film on silicon: **a**) as-synthesized: *full square* and silicon substrate: *line*; **b**) calcined: *empty square* and silicon substrate: *line*; **c**) template extraction with ethanol: *empty circle* and silicon substrate: *line*

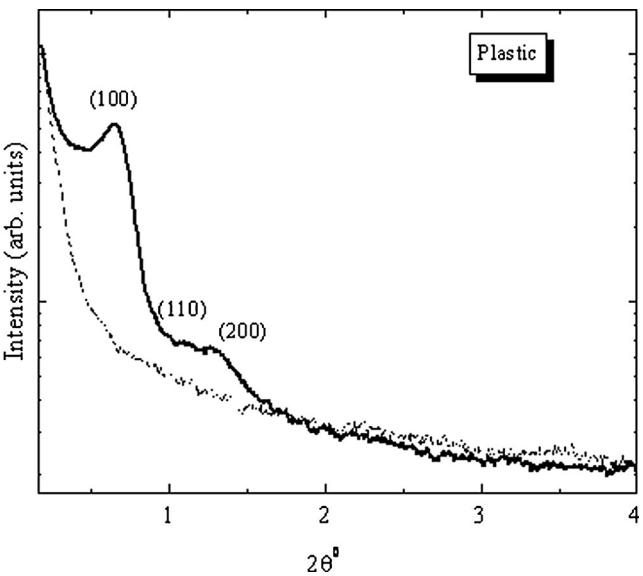

Fig. 6 SAXS Patterns of SBA-15 film on plastic: as-synthesized: *line*, plastic substrate: *dash*

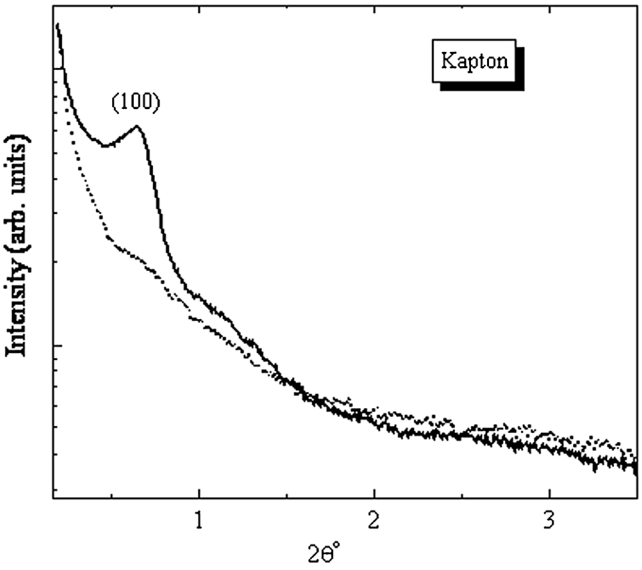

Fig. 7 SAXS Patterns of SBA-15 film on Kapton: as-synthesized: *line*, Kapton substrate: *dash*

the broad bands at higher angles, also indexed as (100) and (200), indicate that smaller mesopores are also formed, probably in regions closer to the surface or to the substrate interface [17].

Figure 5 shows the XRR patterns for films on top of (100) silicon. Before template removal, the (100) and (200) peaks give a=10.7 nm. After calcination, structural shrinkage leads to a=8.9 nm, while after template extraction with ethanol, mild shrinkage was observed, corresponding to a=10.3 nm.

Small-angle X-ray scattering results for the as-synthesized film formed on a commercial plastic substrate are shown in Fig. 6. A well-resolved peak is indexed as (100) reflection and two additional weak peaks correspond to (110) and (200) reflections. These peaks provide a large unit-cell parameter, approximately 15.7 nm. This larger value corresponds to the ordered porous structure with cylinders perpendicular to the substrate, accessible in the transmission geometry, rather than to the ordered porous structure with cylinders parallel to the substrate, examined in the reflection geometry [47]. For mesoporous silica on Kapton polyimide substrate, the SAXS data, Fig. 7, shows only one clear peak, corresponding to the (100) diffraction peak, and yields a cell parameter of 15.7 nm, as observed for the plastic substrate.

Table 2 Lattice parameter (±0.7 nm) of the films, obtained from XRR and SAXS data

Substrate	As-synthesized a/nm	Calcined a/nm	Template extraction a/nm
Glass	11.0[a]	8.0[a]	8.6[a]
Kapton	15.7[b]	–	15.7[b]
Silicon	10.7[a]	8.9[a]	10.3[a]
Stainless steel	10.9[a]	7.1[a]	8.6[a]
Plastic	15.7[b]	–	–
Powder	14.0[b]	11.0[b]	14.0[b]

[a] X-ray reflectivity data ($a_{//}$)

[b] Small-angle scattering transmission data ($a_{\perp}$)

The same lattice parameter, 15.7 nm, was obtained from the mesoporous film on Kapton, from which the template was extracted with ethanol. This result, depicted in Fig. 8, points to no shrinkage.

Table 2 summarizes the lattice parameter results of all analyzed samples. In order to distinguish the lattice parameters for cylinders that are parallel to the substrate from those for cylinders that are perpendicular to it, we will denote them $a_{//}$ and a_{∞}, respectively. The XRR data revealed that the lattice

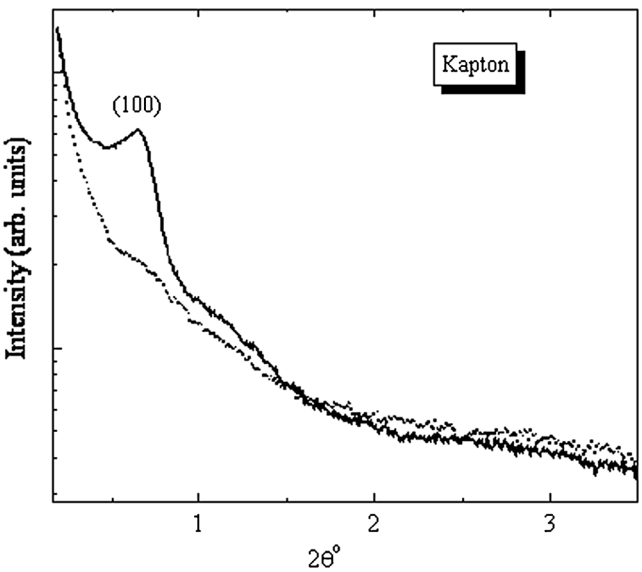

Fig. 8 SAXS Patterns of SBA-15 film on Kapton: template extraction with ethanol: *line*, Kapton substrate: *dash*

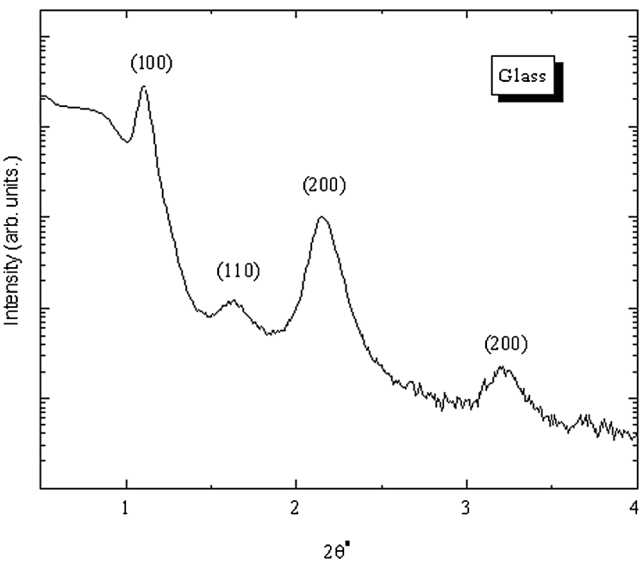

Fig. 9 XRR patterns of SBA-15 film on glass: template extraction with ethanol and with heat treatment at 230 °C

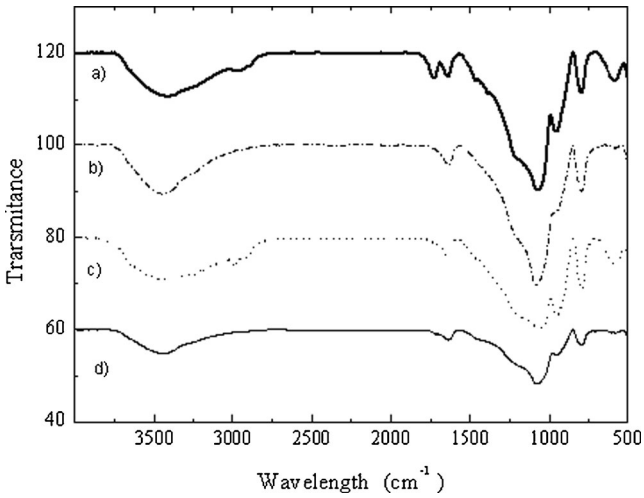

Fig. 10 IR spectra of *a* as-synthesized, *b* calcined, *c* ethanol washed, and *d* ethanol washed and heat treatment SBA-15 films

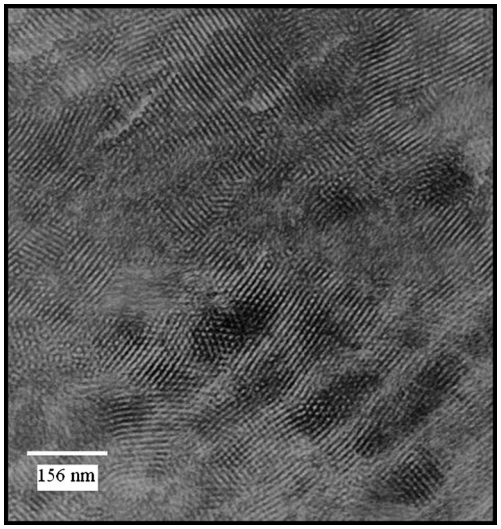

Fig. 12 Transmission electron micrograph of SBA-15 film on stainless steel; solvent extraction with ethanol

parameters of all as-synthesized films are similar. The drying process therefore governs the morphology of the mesoporous structure on substrates that have the same affinity to the sol. The better structured films were obtained on the glass substrate, which has larger surface roughness than (100) silicon. On the other hand, not well-organized mesopores were formed on stainless steel, which possesses the highest surface roughness. Therefore, not only the physical properties of the substrates, but also the dynamic chemical surface-liquid interactions during the drying process govern the morphology of the films, a point already made by Chougnet et al. [30]. Other experiments will have to be carried out in order to separate these two parameters, such as those proposed by the Chougnet et al. [30].

Since the methods used to remove the templates from the as-synthesized SBA-15 films were not efficient, as revealed by the large shrinkage caused by calcination and the presence of polymer remains after ethanol extraction, we have resorted to a new, two-step removal procedure [47]. The polymer template was initially removed by solvent extraction under ethanol flow. Subsequently, the sample was submitted to heat treatment at 230 °C for 4 h.

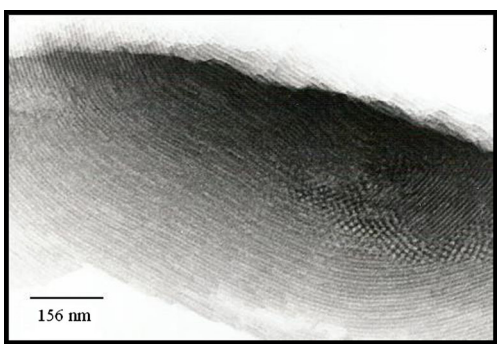

Fig. 11 Transmission electron micrograph of calcined SBA-15 film on a glass slide

The XRR pattern of a film on a glass substrate after this process, shown in Fig. 9, displays peaks that correspond to the (100), (200), and (300) reflections and yields the cell parameter a=9.3 nm. The (110) reflection evidences the occurrence of SBA-15 cylinders that are disordered with respect to the substrate. The (110) peak maximum corresponds to the larger lattice parameter a=11 nm, also in agreement with the SAXS data that yielded larger lattice parameters for cylinders that are not parallel to the substrate surface.

Figure 10 shows the infrared (IR) transmission spectra of the aforementioned films: (a) as-synthesized, (b) calcined, (c) after extraction with ethanol at 80 °C for 12 h, and (d) after heat treatment at 230 °C. A broad band at 3,400/cm is partially caused by the O–H stretching vibration mode of the adsorbed water molecules [10]. Several infrared absorption bands at around 2,850–3,000/cm in the spectra (a) and (c) are due to C–H stretching of the P123 template [48], while in spectrum (b) and (d), these absorptions are not detected [9]. This suggests the efficient removal of the organic template by calcination and by the two-step template removal, while only partial removal is observed after ethanol extraction [48]. The large band at 1,082/cm, with shoulders at ca. 1,240/cm and ca. 750/

Table 3 Lattice parameter (±1.5 nm) of the films, obtained from TEM data

Substrate	Calcined a/nm	Template extraction a/nm
Glass (scratched)	$a_{//}$=7.3	–
	–	–
Glass (pop-off)	$a_{//}$=7.5	$a_{//}$=11.5
	$a_{\perp}$=12.0	$a_{\perp}$=15.9
Stainless steel (scratched)	–	$a_{//}$=12.0
	–	$a_{\perp}$=15.0

cm, due to asymmetric and symmetric stretching vibrations of Si–O–Si, decreased after solvent extraction of the template. On the other hand, the band at 960/cm is stronger, showing the presence of silanol groups Si–OH on the surface of an ethanol-washed film. The band around 1,630/cm is due to the O–H stretching mode of adsorbed water molecules [48]. The IR measurements provide a remarkably clear picture of template removal after the different treatments.

The TEM images of a calcined film on glass in Fig. 11 and of a film whose template was removed with ethanol on steel in Fig. 12 show that the entire substrate surfaces are covered with nanotubes, or cylinders, dispersed into fairly well-ordered hexagonal arrays of mesopores and attests to the long-range crystallographic ordering of the films.

The pore channels are oriented mostly parallel to the substrate surface and a more organized mesostructured film is detected on the glass substrate (Fig. 11), in agreement with the XRR data. The lattice parameters taken from the TEM pictures of these films are listed in Table 3. These lattice parameters are in good agreement with the XRR and SAXS data, also giving $a_{\perp} > a_{//}$. Alberius et al. [22] also reported contraction of the d spacing of cylinders oriented parallel to the substrate, in agreement with our XRR and TEM data.

4 Conclusions

A simple sol-gel synthesis and dip-coating method allow deposition of adherent, well-ordered mesoporous silica films on a variety of substrates under identical conditions. The template extraction by calcination at temperatures around 500 °C causes excessive structural shrinkage, and template extraction with ethanol fails to completely remove the polymer. A two-step process, involving ethanol extraction and mild heat treatment at around 200 °C, is a more effective method, leading to template-free films with less structural shrinkage. After total polymer removal, the films present 342 m^2/g surface area, 0.130 cm^3/g pore volume, and 6.8 nm pore diameter. As pointed out by previous authors [27, 30, 49], the pore structure of the films depends on the substrate and are mostly governed by topological properties, rather than by wetting affinity to the sol. All substrates have similar wetting properties in contact with the alcoholic sol. Rough substrates avoid the alignment of pores parallel to the substrate surface, as evidenced by XRR and TEM data. All prepared films were submitted to the same drying protocol after dip coating; therefore, the results indicate that the morphological features of the substrates govern the pore-structure formation during drying. The pore size depends on the orientation of the pores to the film surface and is smaller for pores parallel to the surface of the substrates, i. e., for their preferred orientation.

Acknowledgments The authors thank Dr. Sylvia M. Carneiro for the TEM images (Laboratório de Biologia Celular do Instituto Butantã) and for the fruitful discussions. Thanks are due to Mr. Marcelo Nakamura and Prof. Henrique E. Toma for the use of the AFM facility. We also acknowledge the financial support of the FAPESP and CAPES. This research was supported by the CNPq under the RHAE/EMBRACO innovation project agreement (50.5002/2004-3). Special acknowledgments are due to EMBRACO and the researchers Ms. Eng. Fabian Fagoti and Dr. Hannes Fischer.

References

1. A. Stein, Microporous Mesoporous Mater. **44**, 227 (2001)
2. H. Minakuchi, K. Nakanishi, N. Soga, N. Ishizuka, N. Tanaka, Anal. Chem. **68**, 3498 (1996)
3. H. Yang, N. Coombs, I. Sokolov, G.A. Ozin, Nature **381**, 589 (1996)
4. A. Tagushi, F. Schüth, Microporous Mesoporous Mater. **77**, 1 (2005)
5. C.T. Kresge, M.E. Leonowicz, W.J. Roth, J.C. Vartulli, J.S. Beck, Nature **359**, 710 (1992)
6. J.S. Beck, J.C. Vartuli, W.J. Roth, M.E. Leonowicz, C.T. Kresg, K.D. Schmitt, C.T.-W. Chu, D.H. Olson, E.W. Sheppard, S.B. McCullen, J.L. Schlenker, J. Am. Chem. Soc. **114**, 10834 (1992)
7. Q. Huo, D.I. Margolese, U. Ciesla, P. Feng, T.E. Gier, P. Sieger, R. Leon, P.M. Petroff, F. Schuth, G.D. Stucky, Nature **368**, 317 (1994)
8. D. Zhao, Q. Huo, N. Melosh, G.H. Fredrickson, B.F. Chmelka, G.D. Stucky, Science **279**, 548 (1998)
9. Z.-L. Hua, J.-L. Shi, L. Wang, W.-H. Zhang, J. Non-Cryst. Solids **292**, 177 (2001)
10. D. Zhao, Q. Huo, J. Feng, B.F. Chmelka, G.D. Stucky, J. Am. Chem. Soc. **120**, 6024 (1998)
11. J. Patarin, Angew. Chemie. Int. Ed. **43**, 3878 (2004)
12. L.P. Mercuri, L. Carvalho, F.A. Lima, C. Quayle, M.C.A. Fantini, G. Tanaka, W. Cabrera, M. Furtado, D.V. Tambourgi, J.R. Matos, M. Jaroniec, O.A. Sant'Anna, Small **2**, 254 (2006)
13. J.M. Bertolo, A. Bearzotti, P. Falcaro, E. Traversa, P. Innocenzi, Sensor Lett **1**, 64 (2003)
14. M. Nath, C.N.R. Rao, J. Am. Chem. Soc. **123**, 4841 (2001)
15. L. Nicole, C. Boissiere, D. Grosso, A. Quach, C. Sanchez, J. Mater. Chem. **15**, 3598 (2005)
16. S.S. Prakash, C.J. Brinker, A.J. Hurd, J. Non-Cryst. Solids **190**, 264 (1995)
17. Y. Lu, R. Ganguli, C.A. Drewien, M.T. Anderson, C.J. Brinker, W. Gong, Y. Guo, H. Soyez, B. Dunn, M.H. Huang, J.I. Zink, Nature **389**, 364 (1997)
18. A. Sellinger, P.M. Weiss, A. Nguyen, Y. Lu, R.A. Assink, W. Gong, C.J. Brinker, Nature **394**, 256 (1998)
19. C.J. Brinker, Y. Lu, A. Sellinger, H. Fan, Adv. Mater. **11**, 579 (1999)
20. D. Zhao, P. Yang, D.I. Margolese, B.F. Chmelka, G.D. Stucky, Chem. Commun. 2499 (1998)
21. N. Nishiyama, A. Koide, Y. Egashira, K. Ueyama, Chem. Commun. 2147 (1998)
22. P.C.A. Alberius, K.L. Friendell, R.C. Hayward, E.J. Kramer, G.D. Stucky, B.F. Chmelka, Chem. Mater. **14**, 3284 (2002)
23. N. Yao, A.Y. Ku, N. Nakagama, T. Lee, D.A. Saville, I.A. Aksay, Chem. Mater. **12**, 1536 (2000)
24. D. Grosso, F. Cagnol, G.J.A.A. Soler-Illia, E.L. Crepaldi, H. Amenitsch, A. Brunet-Bruneau, A. Bourgeois, C. Sanchez, Adv. Funct. Mater. **14**, 309 (2004)
25. R.C. Hayward, P. Alberius-Henning, B.F. Chmelka, G.D. Stucky, Microporous Mesoporous Mater. **44–45**, 612 (2001)
26. G.J.A.A. Soller-Illia, P. Innocenzi, Chem. Eur. J. **12**, 4478 (2006)
27. H. Miyata, K.J. Kuroda, Am. Chem. Soc. **121**, 7618 (1999)

28. H. Miyata, K.J. Kuroda, J. Am. Chem. Mater. **12**, 50 (2000)
29. A. Chougnet, C. Heitz, E. Søndergard, J. Berquier, P. Albouy, M. Klotz, J. Mater. Chem. **15**, 3340 (2005)
30. A. Chougnet, C. Heitz, E. Søndergard, P. Albouy, M. Klotz, Thin Solid Films **495**, 40 (2006)
31. H. Yang, A. Kuperman, N. Coombs, S. Mamiche Afara, G.A. Ozin, Nature **379**, 6567 (1996)
32. H. Yang, N. Combs, I. Sokolov, G.A. Ozin, Nature **381**, 6583 (1996)
33. H. Yang, N. Combs, G.A. Ozin, J. Mater. Chem. **8**, 1205 (1998)
34. H. Miyata, K. Kuroda, Chem. Mater. **11**, 1609 (1999)
35. B.W. Eggiman, M.P. Tate, H.W. Hillhouse, Chem. Mater. **18**, 723 (2006)
36. V.R. Koganti, D. Dunphy, V. Gowrishankar, M.D. McGehee, X. Li, J. Wang, V.R. Rankin, Nanoletters **6**, 2567 (2006)
37. H.W. Hillhouse, J.W. van Egmond, M. Tsapatsis, J.C. Hanson, J.Z. Larese, Microporous Mesoporous Mater. **44–45**, 639 (2001)
38. R. Bandyopadhyaya, E. Nativ-Roth, R. Yerushalmi-Rozen, O. Regev, Chem. Mater. **15**, 3619 (2003)
39. V.V. Guliants, M.A. Carreon, Y.S. Lin, J. Membrane. Sci. **235**, 53 (2004)
40. T. Clark Jr., J.D. Ruiz, H. Fan, C.J. Brinker, B.I. Swanson, A.N. Parikh, Chem. Mater. **12**, 3879 (2000)
41. H. Yang, G. Vovk, N. Coombs, I. Sokolov, G.A. Ozin, J. Mater. Chem. **8**, 743 (1998)
42. H. Yang, N. Coombs, G.A. Ozin, J. Mater. Chem. **8**, 1205 (1998)
43. D. Grosso, A.R. Balkenende, P.A. Albouy, A. Ayral, H. Amenitsch, F. Babonneau, Chem. Mater. **13**, 1848 (2001)
44. P.A. Albouy, A. Ayral, Chem. Mater. **14**, 3391 (2002)
45. M. Klotz, V. Rouessac, D. Rebiscoul, A. Ayral, A. van der Lee, Thin Solid Films **495**, 214 (2006)
46. D. Zhao, J. Feng, Q. Huo, N. Melosh, G.H. Fredrickson, B.F. Chmelka, G.D. Stucky, Science **279**, 548 (1998)
47. R.M. Grudzien, B.E. Grabicka, M. Jaroniec, J. Mater. Chem. **16**, 819 (2006)
48. B. Tian, X. Liu, C. Yu, F. Gao, Q. Luo, S. Xie, B. Tu, D. Zhao, Chem. Commun. 1186 (2000)
49. R.H. Wang, J. Sun, Nanotechnology **18**, 185705 (2007)